Growth mode and atomic structure of MnSi thin films on Si(111)

B. Geisler,[1] P. Kratzer,[1] T. Suzuki,[2,3] T. Lutz,[2] G. Costantini,[2,4] and K. Kern[2,5]

[1]*Fakultät für Physik and Center for Nanointegration (CeNIDE), Universität Duisburg-Essen, 47048 Duisburg, Germany*

[2]*Max-Planck-Institut für Festkörperforschung, 70569 Stuttgart, Germany*

[3]*Department of Electronics Engineering and Computer Science, Fukuoka University, Fukuoka 814-0180, Japan*

[4]*Department of Chemistry, University of Warwick, Coventry, CV4 7AL, United Kingdom*

[5]*Institut de Physique de la Matière Condensée, École Polytechnique Fédérale de Lausanne, CH-1015 Lausanne, Switzerland*

(Received 23 February 2012; published 19 September 2012)

Thin films of MnSi(111) in B20 structure formed by reactive epitaxy on Si(111) are studied using scanning tunneling microscopy (STM) and density functional theory calculations. Coexisting $\sqrt{3} \times \sqrt{3}$ structures with high or low corrugation are observed and assigned to different Mn coverage by using a detailed analysis of simulated STM images. Comparison with our interpretation of STM images of films previously grown by codeposition of Mn and Si provides us with evidence that the stacking sequence of Mn and Si lattice planes depends on the growth protocol.

DOI: 10.1103/PhysRevB.86.115428 PACS number(s): 68.55.−a, 68.35.Md, 68.37.Ef

I. INTRODUCTION

For future spin injection[1,2] into silicon, researchers are seeking magnetic materials that allow them to fabricate well-defined atomically sharp interfaces with the Si substrate. Both theoretical[3] and experimental[4–14] studies have recently shown that MnSi can be grown epitaxially on Si(111) in its ground-state B20 crystal structure. The interest in MnSi has been renewed over the last years, also due to its peculiar magnetic bulk properties.[15–18] For thin films on Si(111), increased ordering temperatures have been reported[10,11] and studies of magnetic anisotropy and magnetic texture under epitaxial strain have been performed.[12,13] However, the atomic structure of the films and their dependence on the growth parameters have remained elusive.[5,6,8,14]

Here we combine scanning tunneling microscopy (STM) experiments of *in situ* prepared MnSi films and density functional theory (DFT) calculations to determine the structure and surface termination of MnSi films and their dependence on the growth conditions.

The MnSi films reported in the literature have been fabricated in two alternative ways: One possibility is the codeposition[6,9,12,14] of Mn and Si (either simultaneously or by alternating atomic-layer deposition) on the Si(111) substrate, followed by an annealing step. With this technique, only moderate mobility of the deposited atoms is required to establish atomic order in the MnSi film. As an advantage, this growth technique yields closed and rather smooth films, possibly with single-layer steps. The second possible route to MnSi films on Si(111) is reactive epitaxy,[4,6–11] depositing solely Mn, again followed by annealing at generally higher temperatures. In this case, the Si atoms required to form the MnSi compound originate from the Si substrate. Under suitably chosen annealing temperatures, the latter technique yields films that are smooth over a wide range but which contain holes (or craters) that allow Si atoms to leave the substrate and diffuse to the film surface. With this technique, the composition and termination of the films is in principle determined by the lowest-energy structure. However, since the experimental annealing temperatures are typically low, nonequilibrium situations can emerge, given that the material transport of Si from the craters to the growth surface may take time due to the limited mobility of Si.

The B20 structure of bulk MnSi [space group $P2_13$, lattice constant $a_0 = 4.56$ Å (Ref. 19)] is a cubic crystal structure with four Mn and four Si atoms in the unit cell that lacks inversion symmetry. Along the [111] direction, the 12-layer repetition period resulting from the B20 structure may be divided into three quad-layers (QLs). In an infinite crystal, each QL has the same internal structure, consisting of a sequence of a Si-dense, Mn-sparse, Si-sparse, and Mn-dense layer, following the terminology introduced in Ref. 3. The three QLs build up the crystal structure via an *A*-*B*-*C*-*A*-*B*-*C*-... stacking. For MnSi films on Si(111), the lack of inversion symmetry of the B20 structure adds to the complexity. From the substrate-film interface upwards, the MnSi film may be grown in two different stacking orientations (cf. Fig. 1): either following the sequence Si-dense, Mn-sparse, Si-sparse, Mn-dense, and so forth (called the "up" stacking in the following), or the inversely ordered sequence, Si-dense, Mn-dense, Si-sparse, Mn-sparse, and so forth (called the "down" stacking in the following). In both cases, we model the bonding of the MnSi film with the substrate to be made by a Si-dense layer in order to minimize the interface energy under the locally Si-rich conditions present at the interface to the substrate.

For surface-sensitive probes as STM it is not easy to discriminate between these two stackings; thus, a subtle analysis of the subsurface layers and their effect on the experimental data is required. In addition, one has to take into account that the surface stoichiometry may differ from the MnSi bulk stoichiometry due to enrichment or depletion of one of the elements near the surface.

II. EXPERIMENTAL AND COMPUTATIONAL DETAILS

In the present study, MnSi films grown by reactive epitaxy have been investigated with a home-built STM operated in ultrahigh vacuum at room temperature. Si substrates were cut from *n*-type P-doped Si(111) wafers (7–13 mΩ cm, Siltronix).

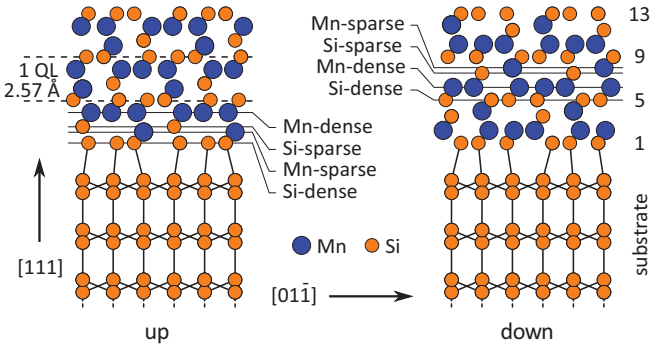

FIG. 1. (Color online) Side views of thin films of MnSi(111) in B20 structure on Si(111), showing "up" (left) and "down" (right) stacking sequence, QL division, internal QL structure, and layer numbering. In the MnSi film, no bonds are displayed for better clarity.

The experimental procedure for preparation of the Si(111) substrates is described elsewhere.[20] One to four monolayers (ML) Mn were deposited onto the clean Si(111)-(7 × 7) surface at room temperature from a Mo crucible heated by electron bombardment. After the Mn deposition, the Si samples were annealed at 300 °C for 15–30 min to form the MnSi films.

Electronic structure calculations of MnSi films on Si(111) were performed in the framework of DFT,[21] using the generalized gradient approximation[22] for electronic exchange and correlations. The plane-wave method was employed (QUANTUMESPRESSO[23]) in conjunction with self-created ultrasoft pseudopotentials,[24] treating the atomic Si $3s$,$3p$ and Mn $3p$,$3d$,$4s$,$4p$ subshells as valence states. For Mn, a nonlinear core correction[25] was included. The spin-polarized calculations were carried out using a supercell approach (Fig. 1): A hexagonal Si(111)-($\sqrt{3} \times \sqrt{3}$) unit cell containing six layers of Si, the MnSi films, and a vacuum region of about 20 Å was used. The lower side of the Si substrate was passivated by H atoms. The lateral cell size was $\sqrt{3/2}\, a_{\mathrm{Si}}^{\mathrm{bulk}} = 6.697$ Å, using the calculated Si lattice constant. The plane-wave cutoffs for wave functions and density were chosen as 35 Ry and 350 Ry, respectively. Brillouin zone sampling was done using a 8 × 8 × 1 Monkhorst-Pack k-point grid[26] and Methfessel-Paxton smearing[27] (5 mRy). The atomic positions were accurately optimized (forces $\leqslant$ 1 mRy/bohr, energy changes $\leqslant$ 0.1 mRy). A dipole correction scheme[28,29] was included, but found to be of minor importance here.

To assess the quality of our pseudopotential approach, we calculated some bulk properties of γ-Mn and B20-MnSi and compared them to all-electron full-potential augmented plane-wave plus local-orbital results.[30] The MnSi lattice constant (4.52 Å vs 4.53 Å) and bulk modulus (208 GPa vs 204 GPa) agree perfectly, as do the magnetic properties. Compared to the experimental value, the calculated lattice constant is only 0.9% too small, which is very good. The same quality of agreement was found for γ-Mn.

The surface energies of the MnSi films, which are accessible via our DFT calculations, allow us to draw further conclusions about the growth modes and their effects on the surface morphology of MnSi films. In the context of *ab initio* thermodynamics,[31] the surface energy depends on a variable

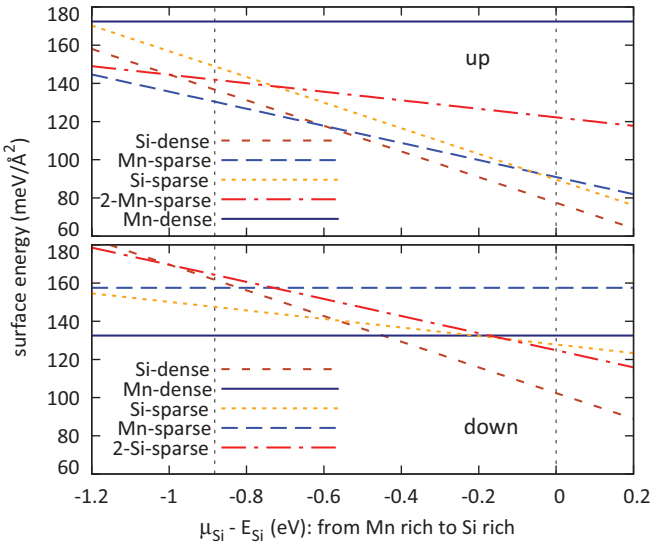

FIG. 2. (Color online) DFT surface energies $\gamma - \gamma_{\mathrm{sub}}$ of MnSi films for various terminations (starting with 13 layers, Si-dense) for up stacking (top) and down stacking (bottom) of the layers. The chemical potential of Si may vary between the Si-poor = Mn-rich (left) or Si-rich (right) growth regimes.

characterizing the chemical environment in which growth takes place. Using the definition

$$\gamma - \gamma_{\mathrm{sub}} = \frac{1}{A}\{E_{\mathrm{slab}} - E_{\mathrm{sub}} - (N_{\mathrm{Si}} - N_{\mathrm{Mn}})\mu_{\mathrm{Si}} - N_{\mathrm{Mn}} E_{\mathrm{MnSi}}\}$$

[where $\gamma_{\mathrm{sub}} \approx 95$ meV/Å^2 is the surface energy of the relaxed bare Si(111) surface, chosen as reference; E_{slab}, E_{sub}, and E_{MnSi} are the DFT total energies of substrate with film, substrate without film, and laterally distorted MnSi bulk, respectively; N_i are the numbers of atoms in the film, excluding the substrate], the chemical potential of Si, μ_{Si}, determines the surface energies. These are displayed in Fig. 2 for various film terminations and for both the up and down stacking of layers. It is important to note here that a so defined "surface energy" γ is actually a combination of the real surface energy and the energy of the interface between the MnSi film and the Si substrate. The individual parts are hard to isolate in our method (due to the missing inversion symmetry of MnSi) and different for the up and the down case. On the other hand, this definition removes the strain energy of the film, caused by epitaxial distortion of the material to the substrate lattice constant, from γ to make terminations of films of different thickness comparable. From the energy difference of laterally (i.e., perpendicular to the [111] direction) distorted and undistorted bulk MnSi the strain energy can be deduced to be 115 meV per formula unit, which translates into a contribution to γ of approximately 12 meV/Å^2 per QL. The vertical dashed lines in Fig. 2 indicate the range of μ_{Si} accessible in equilibrium.[32] In previous work,[3] μ_{Mn} was chosen to characterize the reservoir. Mathematically, both chemical potentials are fully equivalent and can be interchanged via $\mu_{\mathrm{Mn}} = E_{\mathrm{MnSi}} - \mu_{\mathrm{Si}}$. In this work we chose μ_{Si} in the spirit that the amount of Mn is fixed by deposition, but Si is available from the substrate reservoir and thus more variable.

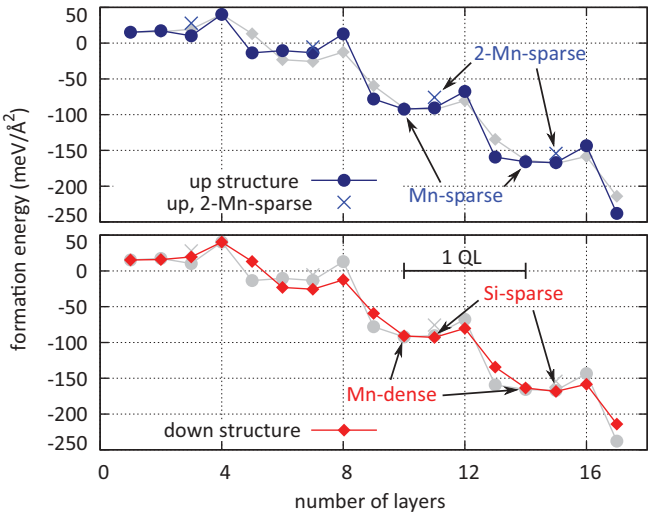

FIG. 3. (Color online) DFT formation energies per area, $E^{\text{form}} - E^{\text{form}}_{\text{sub}}$, for films of up (top) and down (bottom) stacking sequence and different thickness. (For the layer numbering cf. Fig. 1.) The curves clearly exhibit a QL periodicity. The classes of film terminations which we argue to be observed in the experiments are marked.

Additionally and more traditionally,[33–35] film formation energies per area can be considered, which are defined as

$$E^{\text{form}} - E^{\text{form}}_{\text{sub}} = \frac{1}{A}\{E_{\text{slab}} - E_{\text{sub}} - N_{\text{Mn}}E_{\text{Mn}} - N_{\text{Si}}E_{\text{Si}}\}$$

with $E_{\text{Mn/Si}}$ being the diamond-Si and α-Mn[36] bulk total energies. The film formation energies are shown in Fig. 3 for several film thicknesses. Again, the substrate formation energy, $E^{\text{form}}_{\text{sub}} = \gamma_{\text{sub}}$, is chosen as reference. The substrate is always considered to be in equilibrium with Si bulk, therefore γ_{sub} does not depend on a chemical potential variable. Since the formation of MnSi from elemental bulk sources is exothermic, the curves in Fig. 3 have a downward slope on average.

STM images were simulated in the spirit of the Tersoff-Hamann approximation[37,38] for all terminations of MnSi films up to 17 layers in thickness, both for the up and down stacking. For this purpose, the integrated local density of states (ILDOS) was calculated, which is defined as $\sum_{nk} |\psi_{nk}(\mathbf{r})|^2 \delta(\varepsilon_{nk} - \varepsilon)$ integrated over a finite energy interval eV_{bias} above or below the Fermi energy E_{F} for empty-state or filled-state images, respectively. Subsequently, the height above the surface where the ILDOS equals a chosen critical density ρ_{c} was determined and plotted.

III. FILMS FORMED BY REACTIVE EPITAXY

A large-scale STM image of a MnSi film is shown in Fig. 4. Obviously, two different surface terminations are coexistent (in addition to the well-known QL terrace structure[6–8]) leading to high corrugated (HC) and low corrugated (LC) areas in the image. The LC regions always appear in a higher layer above the HC regions ($\Delta z \approx 0.4$ Å) within the corresponding QL. Magnified sections of either region are shown in Fig. 5. The HC areas display isolated, bright protrusions ordered on a hexagonal lattice with distances compatible with the Si(111)-($\sqrt{3} \times \sqrt{3}$) surface lattice constant in the filled-state

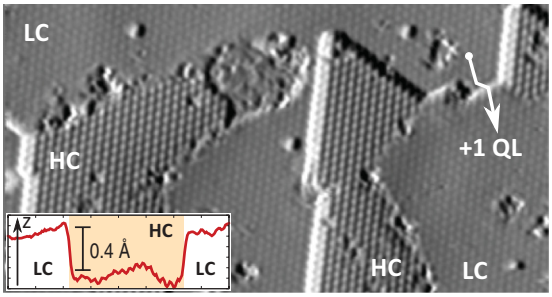

FIG. 4. (Color online) STM image (derivative) taken at a tunneling current of 0.2 nA and a bias voltage of −1.8 V from a MnSi film prepared by deposition of 3.8 ML Mn followed by annealing at $T = 300\,^{\circ}$C for 30 min. The size is 39×26 nm^2. The inset shows an averaged height profile of differently corrugated adjacent areas (belonging to the same QL) to illustrate the height difference.

images. In addition, irregularly distributed triangular features are sometimes observed (not shown here), which are probably due to adatoms.

While comparing the simulated to the experimental images, the goal is to find a *pair* of consecutive surface terminations that matches the HC and LC structures, respectively. In order to determine the best match, we used both filled-state and empty-state images and derived relative heights of the maxima as well as the corrugation (difference between maximum and

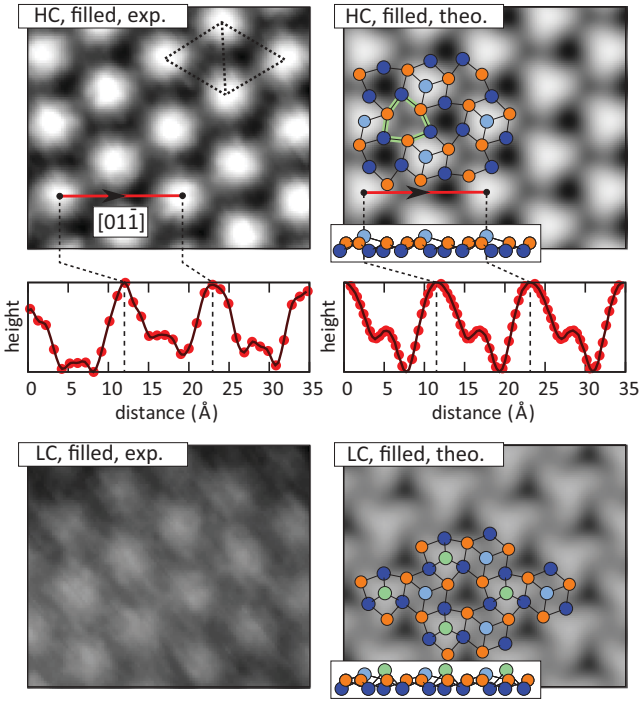

FIG. 5. (Color) Experimental (left column) filled-state STM images and line scans of MnSi HC (upper and middle row) and LC (lower row) surface areas which are compared to data derived from the DFT electronic structure using $V_{\text{bias}} = -1.5$ V for HC and $V_{\text{bias}} = -1.4$ V for LC (right column; $\rho_{\text{c}} = 10^{-5}$/bohr^3). A part of the atomic structure is overlaid: Smaller orange circles mark Si atoms; bigger blue and greenish circles mark Mn atoms. The insets show side views of the film atomic structures (cf. Fig. 1). The dotted parallelogram indicates the unit cell.

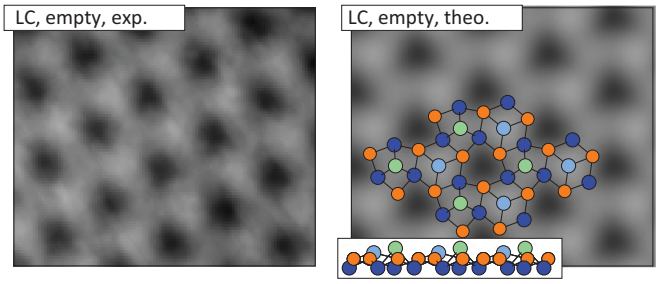

FIG. 6. (Color) Experimental (left) empty-state STM image of a MnSi LC surface area compared to data derived from the DFT electronic structure using $V_{\text{bias}} = +1.2$ V and $\rho_c = 10^{-5}/\text{bohr}^3$ (right).

minimum) for the terminations shown in Fig. 1 as well as several nonstoichiometric ones.

The simulated STM images show a particularly high corrugation for the surface formed by a Mn-sparse layer on top of a Si-dense subsurface layer, being part of the up stacking sequence. This MnSi termination has the lowest surface energy under Mn-rich conditions. The bright spots then represent single Mn atoms (Fig. 5, top row). Interestingly, a line scan along the long diagonal of the unit cell shows additional, smaller maxima at the midpoint between the bright features, which are also observed in our experimental line scans. These appear due to rings (marked green in Fig. 5, top right) formed by Si-dense and Mn-dense atoms in the subsurface layers, centered around the Mn-sparse atom one QL below.

For the LC areas, agreement with experiment is achieved by placing another Mn atom on the HC surface, i.e., by a "2-Mn-sparse" termination (Fig. 5, bottom row). It corresponds to a Si-sparse surface (following Mn-sparse in the up stacking) with the topmost Si atom *replaced* by Mn. As a peculiar feature, the bright spots in the filled-state STM image are transformed into a connected, honeycomblike pattern in the empty-state images (Fig. 6), in agreement with experiment. While our calculations indicate LC for all dense surface terminations, this feature is characteristic for the 2-Mn-sparse termination. This nonstoichiometric surface is higher in surface energy than Si-dense, but may be realized under nonequilibrium conditions during growth. We note that assigning the LC areas to a Si-sparse layer (*without* replacement by Mn) would be inconsistent with its very strong corrugation in the simulations and with the experimentally observed fact that LC regions expand as the Mn coverage is increased.

IV. FILMS FORMED BY CODEPOSITION OF Mn AND Si

Interestingly, the analysis presented here can also be used to demonstrate that the film structure may be significantly different for other growth protocols used in the literature. For MnSi films fabricated by codeposition, Azatyan *et al.* (Ref. 14) recently also reported on the coexistence of smooth and corrugated regions, but with deviations from our observations. First, their line scan [shown in Fig. 5(c) in Ref. 14] severely differs from our experimental line scans. Especially, the height order of HC and LC is reversed, and the HC valleys are even deeper than the LC valleys. Second, from their analysis of the two surface terminations [Fig. 5(b) in Ref. 14] one can deduce that HC is indeed *one* layer *above* LC: If one centers their superposed grid on the LC peaks, it becomes obvious that the HC peaks always appear in the center of those triangles that also contain the deepest minima of the LC region, which (as we know from simulations) correspond to the crystallographical adsorption sites of the next layer. Third, the "honeycomb transition" is not seen at all in Fig. 3 in Ref. 14.

A comparison with our simulated STM images questions the previous structural assignments of Ref. 14. First, their HC areas cannot be assigned to the Si-dense termination of the up stacking due to the weak corrugation obtained from our calculations. Moreover, simulated line scans along the long diagonal of the unit cell show clear secondary maxima between the main peaks that are absent in the experiment [cf. Fig. 5(c) in Ref. 14]. Second, the assignment of LC areas (observed *below* the HC areas by Azatyan *et al.*) to the Mn-dense termination appears unlikely because of the high surface energy of Mn-dense in up stacking (cf. Fig. 2, top panel). We are able to reconcile their images with our calculations only if we assume the down stacking in their films. Then, their HC STM images best match with our simulated images of a Si-sparse layer on a Mn-dense subsurface layer, the latter corresponding to the LC regions. In this case, the bright spots in the HC (LC) images are due to the dangling bonds of single Si atoms (the Mn trimers being seen as one single spot). Simulated STM images of this assignment are shown in Fig. 7. The absence of the honeycomb transition in our simulations strengthens our interpretation: The LC peaks are distinct and invariant under bias voltage reversal. Comparing the absolute height of minima and maxima of our simulated HC and LC images, we find that the HC maxima are above the LC maxima, while the HC minima are below the LC minima, in accordance with Azatyan's observations (cf. Fig. 7, lower row). The shoulders of the HC maxima result from Mn trimers in the Mn-dense layer below.

V. ADATOM LAYER ADSORPTION STABILITY

We also performed a theoretical study of the adsorption of Mn and Si adatom layers on MnSi films to answer the question whether the adatom positions in (a) the 2-Mn-sparse termination (Fig. 5, bottom row and Fig. 6) and (b) the Si-sparse on Mn-dense termination (Fig. 7, right column) are energetically preferable to other possible adsorption sites. Our calculations clearly show that other arrangements of the surface atoms than those already presented are energetically unfavorable and thus quite improbable.

We define the adsorption energy as

$$\varepsilon = E_{\text{slab}} - E_{\text{sub}} - N_{\text{Mn}} E^{\text{atom}}_{\text{Mn}} - N_{\text{Si}} E^{\text{atom}}_{\text{Si}},$$

where E_{slab}, E_{sub}, and $E^{\text{atom}}_{\text{Mn/Si}}$ are the total energies of the film structure with adsorbate, the reference film structure, and the isolated atomic elements, respectively; $N_{\text{Mn/Si}}$ are the numbers of adsorbed Mn and Si atoms. Thus, ε is the adsorption energy per unit cell, which, in our case, includes one or two adsorbed atoms.

The up-Si-dense terminating layer has three principal adsorption sites which we call A, B, and C with increasing Si-Si distance in the surrounding Mn-Si rings (Fig. 8, upper row). In the case of a Mn-sparse termination, according to

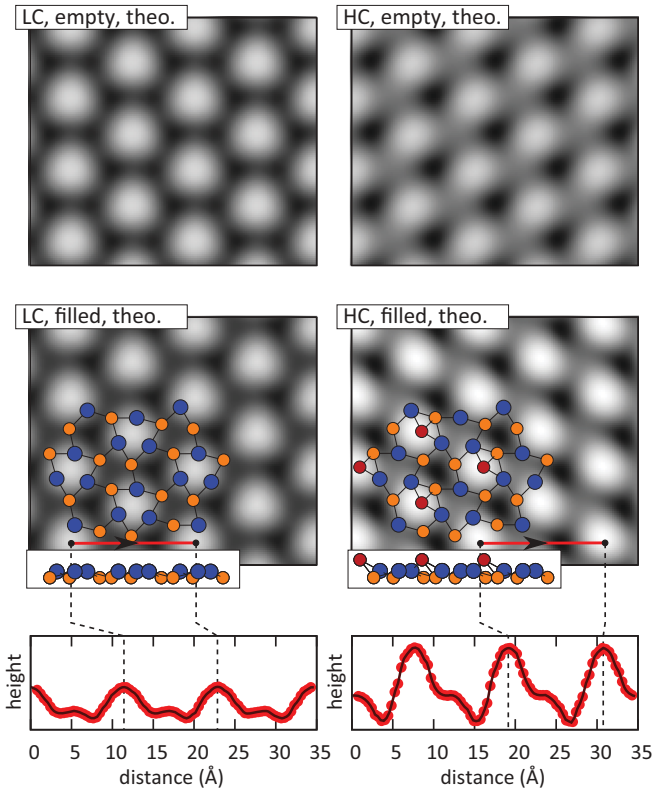

FIG. 7. (Color) Simulated empty-state (upper row) and filled-state (middle row) STM images from the down-stacked LC (left column) and HC (right column) MnSi film structures ($V_{\text{bias}} = \pm 1.2$ V, $\rho_c = 10^{-6}/\text{bohr}^3$). The lower row shows line scans of the simulated LC and HC filled-state images. In the overlaid atomic structures, smaller orange and red circles mark Si atoms; bigger blue circles mark Mn atoms. Again, the insets show side views of the film atomic structures (cf. Fig. 1). The contrast of the LC images has been increased to provide better clarity.

the crystal structure, site B is occupied by a Mn atom. An additional Mn atom can now occupy site C (which would be the 2-Mn-sparse case) or site A. Furthermore, a rearrangement of the Mn atoms to sites A *and* C could be possible, leaving site B unoccupied. However, total energy calculations (Table I) show a clear preference of the 2-Mn-sparse configuration $B + C$.

Analogously, the down-Mn-dense terminating layer also has three principal adsorption sites which we again call A, B, and C (Fig. 8, lower row). Site B corresponds again to the Si adsorption site that continues the crystal structure. We find a significant preference of site B over sites A and C (Table II). Interestingly, the center of site B proves to be unstable: The Si atom moves close to two of the three surrounding Mn atoms, shifting charge from its p_z orbital (perpendicular to the surface) into the lateral p_x and p_y orbitals and reducing the energy by 0.1 eV.

TABLE I. Adsorption energies ε of Mn atoms on the up-Si-dense surface (cf. Fig. 8, upper row). ΔE is given relative to configuration $B + C$. Configurations $A + B$ and $B + C$ can alternatively be interpreted as single-Mn-adatom layer on the Mn-sparse surface termination.

Sites	Adsorption energy/eV: 1 Mn/Mn-sparse	Adsorption energy/eV: 2 Mn/Si-dense	ΔE/eV
Up stacking, 13 layers (Si-dense) + 2 Mn layers			
$A + B$	2.73	6.73	0.58
$A + C$	–	6.77	0.54
$B + C$	3.31	7.31	0.00

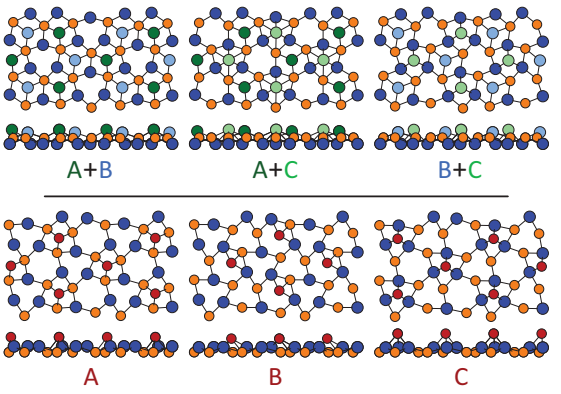

FIG. 8. (Color) Top and side views of structurally optimized adatom layers on different MnSi(111) surface terminations. Upper row: Mn atoms on the up-Si-dense surface. The light blue circles depict adsorbed Mn atoms belonging to the subsequent Mn-sparse layer (site B), whereas dark green and light green atoms represent Mn atoms sitting on the noncrystallographic adsorption positions (sites A and C, as in Figs. 5 and 6). Configuration $B + C$ corresponds to the 2-Mn-sparse case discussed before. Lower row: Si atoms (red circles) on the down-Mn-dense surface. Site B corresponds to the Si-sparse termination.

In Ref. 14, Fig. 6, additional Si was deposited on the HC area at room temperature without further annealing. Our calculations show that, on the down-Si-sparse surface, site C would be occupied by an additional Si atom with an energy preference of about 0.2 eV over site A. Due to the tightness of the underlying Mn triangle, the Si adatom at this position sits 0.6 Å higher than the Si-sparse atom at site B (similar to Fig. 8, lower row, site C). We calculated STM images for this structure and found discrete peaks at the Si adatom position and no qualitative differences between filled- and empty-state images. The STM height difference between the Si-sparse atom peak and the Si adatom peak is even $\approx$0.8 Å. Hence, there are no electronic effects "hiding" the adatom or lowering the contrast, and the adatom (or adatom layer) should be clearly visible in experimental STM images. This agrees with Ref. 14.

TABLE II. Adsorption energies ε of a Si atom on the down-Mn-dense surface (cf. Fig. 8, lower row). ΔE is given relative to site B. The energy of a laterally fixed atom at the center of site B is also shown.

Site	Adsorption energy/eV	ΔE/eV
Down stacking, 14 layers (Mn-dense) + 1 Si layer		
A	4.44	0.36
B (center)	4.70	0.10
B	4.80	0.00
C	4.51	0.29

VI. DISCUSSION

The structures grown by codeposition and by reactive epitaxy show clear differences: In the HC areas, the former have asymmetric peaks, while the latter show strong main peaks with smaller maxima in between (cf. Fig. 5, line scans). This difference in the peak profile results from the different trimer sizes of the underlying layers (the Mn trimers in down stacking are smaller than the Si trimers in up stacking) and from the different atomic species involved. For this reason, the structures of Azatyan *et al.* must be interpreted as down structures different from the up structures fabricated by us. Furthermore, the STM pattern for the down Mn-dense termination is nearly invariant under bias voltage reversal: The honeycomb transition, which arises due to different contributions to the tunneling current from the Mn atoms in the 2-Mn-sparse structure (depending on the applied bias voltage), does not occur here.

Taking into account the surface energies γ, the observed terminations teach us about the prevailing growth conditions: It appears that the films are grown under quite Mn-rich conditions in our experiments, corresponding to the left side of the plots in Fig. 2. Here, the Mn-sparse termination in up stacking is lowest in energy, consistent with its observation in the HC regions. Adding more Mn yields the 2-Mn-sparse structure in the LC regions that is only by about 10 meV / Å^2 higher in energy. The Si-dense termination, which lies energetically between them, is not observed in our experiments. We suspect that the availability of Si is low: Although the films are not closed and Si atoms from the substrate can diffuse to the surface, their diffusion is too slow to establish a Si-dense layer during the annealing period used in film preparation. Thus, μ_{Si} should be interpreted as an effective, "local" chemical potential modeling the quasiequilibrium in certain surface regions, not the equilibrium of the total structure with the Si substrate. In the case of codeposition of Mn and Si, the diffusion of Si from the substrate is not necessary. For the down stacking, the films will mostly be terminated by Si-dense or Mn-dense, depending again on the local value of the chemical potential.[39] The observed Mn-dense termination is favored for $\mu_{\mathrm{Si}} - E_{\mathrm{Si}} < -0.45$ eV. A surface slightly enriched in Si may be realized by terminating the down stacking with a Si-sparse layer, which has the second-best surface energy under Mn-rich conditions.

Moreover, from the formation energies E^{form} shown in Fig. 3 conclusions about the film evolution during growth can be drawn. Superimposed on the overall downward slope, there are structures displaying the QL periodicity. We expect a tendency for growth to stop before the local maxima in E^{form}. These correspond to the Mn-dense and Mn-sparse termination for the up and down stacking, respectively. The idea that kinetic barriers have to be overcome after completion of each fourth layer is consistent with the QL structure of the films observed in our experiments as well as in previous studies.[5,6,8] The local minima of E^{form} are in line with the film terminations experimentally observed: For the down stacking, the Si-sparse and Mn-dense termination locally have the lowest and second-lowest E^{form}. For the up stacking, the local minima of E^{form} occur for Mn-sparse and Si-sparse terminations. This again agrees with the observed structures, if one takes into account that the (energetically only slightly higher) 2-Mn-sparse structure is formed instead of Si-sparse due to lack of available Si atoms. Moreover, Fig. 3 explains why MnSi films consisting of only one QL are rarely observed in experiments:[5,6,8] Film formation from the chemical elements is endothermic ($E^{\mathrm{form}} - E^{\mathrm{form}}_{\mathrm{sub}} > 0$) for these very thin films.

Even though the surface energies and the formation energies are consistent with our structural assignments, it should be emphasized that these concepts are strictly valid only for systems in thermodynamic equilibrium. For Si, GaAs, or GaN, for example (which are typically grown at temperatures between 550 °C and 750 °C, so that material, e.g., As, desorbs into the gas phase[40–42]), this type of description is close to reality. For the growth of epitaxially strained MnSi films on Si(111), the situation is different, although thermodynamic reasoning can still serve as a guideline: The thin films are metastable structures, since $\gamma - \gamma_{\mathrm{sub}}$ is always positive and, as a consequence, Volmer-Weber-like island formation is preferred. This metastability restricts the growth temperatures to quite low values of only about 300 °C in order to *prevent* MnSi from forming islands[3,6,8] instead of thin films. Our calculated DFT adsorption energies ε of Mn and Si atoms on (all) MnSi(111) surfaces are, however, in the range of 3–6 eV per atom. Thus, equilibrium between the film structure and the gas phase cannot be established. Since the low temperatures also reduce the atomic mobility on the surface, a "global" equilibrium of film and substrate is hard to achieve (as stated above) and the appearance of coexisting patches showing different surface terminations with comparable energy becomes quite probable.

VII. CONCLUSION

In summary, MnSi films have been grown by reactive epitaxy on Si(111), and their atomic structures have been characterized by STM and compared to film morphologies obtained with other growth techniques. A detailed comparison using simulated STM images obtained from DFT calculations enabled us to identify the atomic structures of the films, and led us to the conclusion that our films differ in the stacking sequence of the Mn and Si layers from samples grown previously using codeposition of Mn and Si. Independent of the stacking, we have shown that the high and low corrugated surface regions of the MnSi films observed in the experimental STM images correspond to terminations by a layer of single atoms, or by layers containing several Mn atoms per unit cell, respectively. Since the magnetic properties of MnSi films are closely related to their atomic structure,[12] the occurrence of two possible stacking sequences implies that strict control of the growth conditions is required to reproducibly fabricate MnSi films with specified properties.

ACKNOWLEDGMENTS

B.G. and P.K. acknowledge financial support by Deutsche Forschungsgemeinschaft (DFG) within the collaborative research project SFB 491.

[1]G. A. Prinz, Science **282**, 1660 (1998).
[2]S. A. Wolf, D. D. Awschalom, R. A. Buhrman, J. M. Daughton, S. von Molnár, M. L. Roukes, A. Y. Chtchelkanova, and D. M. Treger, Science **294**, 1488 (2001).
[3]M. Hortamani, P. Kratzer, and M. Scheffler, Phys. Rev. B **76**, 235426 (2007).
[4]A. Kumar, M. Tallarida, M. Hansmann, U. Starke, and K. Horn, J. Phys. D: Appl. Phys. **37**, 1083 (2004).
[5]S. Higashi, Y. Ikedo, P. Kocan, and H. Tochihara, Appl. Phys. Lett. **93**, 013104 (2008).
[6]S. Higashi, P. Kocán, and H. Tochihara, Phys. Rev. B **79**, 205312 (2009).
[7]J. Hirvonen Grytzelius, H. M. Zhang, and L. S. O. Johansson, Phys. Rev. B **78**, 155406 (2008).
[8]J. Hirvonen Grytzelius, H. M. Zhang, and L. S. O. Johansson, Phys. Rev. B **80**, 235324 (2009).
[9]E. Magnano, E. Carleschi, A. Nicolaou, T. Pardini, M. Zangrando, and F. Parmigiani, Surf. Sci. **600**, 3932 (2006).
[10]E. Magnano, F. Bondino, C. Cepek, F. Parmigiani, and M. C. Mozzati, Appl. Phys. Lett. **96**, 152503 (2010).
[11]E. Karhu, S. Kahwaji, T. L. Monchesky, C. Parsons, M. D. Robertson, and C. Maunders, Phys. Rev. B **82**, 184417 (2010).
[12]E. A. Karhu, S. Kahwaji, M. D. Robertson, H. Fritzsche, B. J. Kirby, C. F. Majkrzak, and T. L. Monchesky, Phys. Rev. B **84**, 060404 (2011).
[13]E. A. Karhu, U. K. Rößler, A. N. Bogdanov, S. Kahwaji, B. J. Kirby, H. Fritzsche, M. D. Robertson, C. F. Majkrzak, and T. L. Monchesky, Phys. Rev. B **85**, 094429 (2012).
[14]S. Azatyan, O. Utas, N. Denisov, A. Zotov, and A. Saranin, Surf. Sci. **605**, 289 (2011).
[15]C. Pfleiderer, D. Reznik, L. Pintschovius, H. von Löhneysen, M. Garst, and A. Rosch, Nature (London) **427**, 227 (2004).
[16]C. Pfleiderer, S. R. Julian, and G. G. Lonzarich, Nature (London) **414**, 427 (2001).
[17]S. Mühlbauer, B. Binz, F. Jonietz, C. Pfleiderer, A. Rosch, A. Neubauer, R. Georgii, and P. Böni, Science **323**, 915 (2009).
[18]F. Jonietz, S. Mühlbauer, C. Pfleiderer, A. Neubauer, W. Münzer, A. Bauer, T. Adams, R. Georgii, P. Böni, R. A. Duine, K. Everschor, M. Garst, and A. Rosch, Science **330**, 1648 (2010).
[19]J. E. Jørgensen and S. E. Rasmussen, Powder Diffr. **6**, 194 (1991).
[20]T. Suzuki, T. Lutz, D. Payer, N. Lin, S. L. Tait, G. Costantini, and K. Kern, Phys. Chem. Chem. Phys. **11**, 6498 (2009).
[21]W. Kohn and J. L. Sham, Phys. Rev. **140**, A1133 (1965).
[22]J. P. Perdew, K. Burke, and M. Ernzerhof, Phys. Rev. Lett. **77**, 3865 (1996).
[23]P. Giannozzi *et al.*, J. Phys.: Condens. Matter **21**, 395502 (2009).
[24]D. Vanderbilt, Phys. Rev. B **41**, 7892 (1990).
[25]S. G. Louie, S. Froyen, and M. L. Cohen, Phys. Rev. B **26**, 1738 (1982).
[26]H. J. Monkhorst and J. D. Pack, Phys. Rev. B **13**, 5188 (1976).
[27]M. Methfessel and A. T. Paxton, Phys. Rev. B **40**, 3616 (1989).
[28]L. Bengtsson, Phys. Rev. B **59**, 12301 (1999).
[29]B. Meyer and D. Vanderbilt, Phys. Rev. B **63**, 205426 (2001).
[30]P. Blaha, K. Schwarz, G. K. H. Madsen, D. Kvasnicka, and J. Luitz, WIEN2K, *an Augmented Plane Wave + Local Orbitals Program for Calculating Crystal Properties* (Techn. Univ. Wien, Austria 2001).
[31]K. Reuter, C. Stampfl, and M. Scheffler, in *Handbook of Materials Modeling*, edited by D. Yip (Kluwer, Dordrecht, 2004).
[32]Since the validity of thermodynamic considerations should not be overestimated here, as discussed more deeply below, the inserted lines serve more as reference points than as absolute limits.
[33]H. Wu, M. Hortamani, P. Kratzer, and M. Scheffler, Phys. Rev. Lett. **92**, 237202 (2004).
[34]H. Wu, P. Kratzer, and M. Scheffler, Phys. Rev. B **72**, 144425 (2005).
[35]M. Hortamani, H. Wu, P. Kratzer, and M. Scheffler, Phys. Rev. B **74**, 205305 (2006).
[36]We derive the total energy of bulk α-Mn (which is the ground-state crystal structure of Mn, but quite complicated) by calculating antiferromagnetic γ-Mn (fcc structure) and correcting (Ref. 43) the resulting energy by -0.07 eV per formula unit.
[37]J. Tersoff and D. R. Hamann, Phys. Rev. Lett. **50**, 1998 (1983).
[38]J. Tersoff and D. R. Hamann, Phys. Rev. B **31**, 805 (1985).
[39]We note, however, that in the case of closed films, the surface termination will depend more strongly on the deposited Mn and Si coverages than in the case of reactive epitaxy.
[40]C. T. Foxon, J. Vac. Sci. Technol. B **1**, 293 (1983).
[41]W. Theis and R. M. Tromp, Phys. Rev. Lett. **76**, 2770 (1996).
[42]E. J. Tarsa, B. Heying, X. H. Wu, P. Fini, S. P. DenBaars, and J. S. Speck, J. Appl. Phys. **82**, 5472 (1997).
[43]D. Hobbs and J. Hafner, J. Phys.: Condens. Matter **13**, L681 (2001).